Hindawi Publishing Corporation
Journal of Nanomaterials
Volume 2007, Article ID 48247, 10 pages
doi:10.1155/2007/48247

Research Article

Luminescence, Energy Transfer, and Upconversion Mechanisms of Y_2O_3 Nanomaterials Doped with Eu^{3+}, Tb^{3+}, Tm^{3+}, Er^{3+}, and Yb^{3+} Ions

TranKim Anh,[1] Paul Benalloul,[2] Charles Barthou,[2] Lam thiKieu Giang,[1] Nguyen Vu,[1] and LeQuoc Minh[1,3]

[1] *Institute of Materials Science, Vietnamese Academy of Science and Technology, 18 Hoang Quoc Viet Road, Cau Giay, Hanoi, Vietnam*
[2] *Institute des Nanosciences de Paris (INSP), UMR-CNRS 7588, Universites Pierre et Marie Curie et Denis Diderot, 140 Rue de Lourmel, Paris 75015, France*
[3] *College of Technology, Vietnam National University, 144 Xuan Thuy Street, Cau Giay District, Hanoi, Vietnam*

Received 21 May 2007; Revised 16 December 2007; Accepted 31 December 2007

Recommended by Wieslaw Strek

Luminescence, energy transfer, and upconversion mechanisms of nanophosphors ($Y_2O_3 : Eu^{3+}$, Tb^{3+}, $Y_2O_3 : Tm^{3+}$, $Y_2O_3 : Er^{3+}$, Yb^{3+}) both in particle and colloidal forms were studied. The structure, phase, and morphology of the nanopowders and nanocolloidal media were determined by high-resolution TEM and X-ray diffraction. It was shown that the obtained nanoparticles have a round-spherical shape with average size in the range of 4 to 20 nm. Energy transfer was observed for $Y_2O_3 : Eu^{3+}$, Tb^{3+} colloidal and powders, upconversion transitions were observed for both $Y_2O_3 : Er^{3+}$ and $Y_2O_3 : Er^{3+}$, Yb^{3+} nanophosphors. The dependence of photoluminescence (PL) spectra and decay times on doping concentration has been investigated. The infrared to visible conversion of emission in $Y_2O_3 : Er^{3+}$, Yb^{3+} system was analyzed and discussed aiming to be applied in the photonic technology.

1. INTRODUCTION

Luminescent nanomaterials in the form of nanoparticles, nanorods, nanowires, nanotubes, as well as colloidal or bulk nanocrystals are of interest not only for basic research, but also for interesting application [1–3]. High surface to volume ratio, local phenomena such as absorption or change in the surface electronic state may contribute significantly to special properties. An understanding of luminescent properties, energy transfer (ET), and upconversion could determine how to tailor nanophores for a given application. Nanomaterials have potential application as efficient display phosphors, such as in new flat panel displays with low-energy excitation source [2, 3]. Y_2O_3:Eu^{3+} phosphor, one of the most promising oxides-based red phosphors, was studied for a long time because of its efficient luminescence under ultraviolet (UV) and cathode-ray excitation. Y_2O_3:Eu^{3+} with micrometer size grains was used as the red component in three chromatic lamps and projection color television [4–6]. Numerous studies were focused on synthesis and optical properties of nanosized Y_2O_3:Eu^{3+} phosphors [7–10]. Size-dependence efficiency in Y_2O_3:Tb^{3+} [11] and effect of grain size on wavelength of Y_2O_3:Eu^{3+} [12] were investigated. Different methods were used to prepare Y_2O_3:RE^{3+} nanocrystals [13–19] such as chemical vapor synthesis [15], combustion [16, 17], sol-gel [18], and aerosol pyrolysis [19]. Relationship between optical properties and crystalline of nanometer Y_2O_3:Eu^{3+} phosphor has been investigated [20]. The new method of polyol-mediated synthesis of nanoscale materials was presented [21, 22] and the luminescence properties of nanocrystalline Y_2O_3:Eu^{3+} were investigated [23]. Anh et al. studied the ET between Tb^{3+} and Eu^{3+} in Y_2O_3 microcrystals [4]. The role of the active center concentrations in the ET of lanthanide ions was investigated not only for Y_2O_3:Tb^{3+}, Eu^{3+}, but also for organic compound glutamic acid as well as LnP_5O_{14} laser crystals [24]. ET and relaxation processes in Y_2O_3:Eu^{3+} were studied [25]. Preparation and optical spectra of trivalent rare earth ions doped cubic Y_2O_3 nanocrystal have received our considerable attention over 10 years [10, 16, 26–33]. Not only the Eu^{3+}-Tb^{3+} couple, but also the Er^{3+}-Yb^{3+} one are attractive for application in visible emission by ET and upconversion processes. Among emission properties of Y_2O_3 doped with rare earth ions, upconversion is the most attractive phenomenon not only from

photophysic mechanism, but also for application. The enhancement of the red emission via upconversion in bulk and nanocrystalline cubic $Y_2O_3:Er^{3+}$ has been studied [34]. Red, green, and blue upconversion luminescences of trivalent rare earth ion doped Y_2O_3 nanocrystals were investigated [35]. Effect of Yb^{3+}codoping on the upconversion luminescence properties of $Y_2O_3:Yb^{3+}$, Er^{3+} nanocrystallines and nanostructures have been studied [36–38]. The absorption and emission spectroscopy of Er^{3+}-Yb^{3+} doped aluminum oxide waveguides were reported [39].

The oxide lattice has proved to be an excellent host material for some of the most powerful laser built. Among them, Y_2O_3 is characterized by low-phonon frequencies which make inefficient nonradiative relaxation of the excited states. The Y_2O_3 host was chosen due to its high refractory properties with a melting point of about 2450°C, a very high thermal conductivity of 33 W m^{-1} K^{-1}, and a density of 5.03 g cm^3. Y_2O_3 is a suitable material for photonic waveguide due to its high-energy band gap of 5.8 eV, a high refractive index about 2, and a wide transmission region from 280 nm to 8 micrometer. Eu^{3+} exhibits an atomic-like transition in red region at 612 nm. Er^{3+} emissions lie in infrared around 1530 nm as well as upconversion in visible ranges of green and red. The blue emission of Tm^{3+} ions is one of the three important basic colors of display. However, up to now, few articles were devoted to Y_2O_3 doped with Tm^{3+} and codoped with Tb^{3+}, Eu^{3+} or Yb^{3+}, Er^{3+} in both the nanopowder or nanocolloidal forms.

In this work, we report on new synthesis of Y_2O_3 nanophosphor in the two forms of powders and colloidal doped with Tb^{3+}, Eu^{3+}, Tm^{3+}, Er^{3+}, and Yb^{3+}. The concentration dependence and the influence of size on the luminescent properties will be discussed. The investigation of ET between Tb^{3+} and Eu^{3+}, and the mechanism of upconversion in $Y_2O_3:Er^{3+}$, Yb^{3+} nanosize are of the main points.

2. EXPERIMENT

The powder nanophosphors $Y_2O_3:Eu^{3+}$ (1–10 mol%), $Y_2O_3:Er^{3+}$ (1–15 mol%) and $Y_2O_3:Er^{3+}$ (1 mol%), Yb^{3+} (5%), and $Y_2O_3:Tm^{3+}$ (1–4 mol%) were prepared by combustion reaction. Europium oxide (99.995%, CERAC), Yttrium oxide (99.999%, ALFA), and nitric acid and urea (99%, SIGMA-ALDRICH) were used as starting raw materials to prepare $Y_2O_3:Eu^{3+}$. $Y(NO_3)_3$ and $RE(NO_3)_3$ stock solutions were prepared by dissolving Y_2O_3, Er_2O_3, Yb_2O_3, and Eu_2O_3 in nitric acid and diluting with deionized water. The synthesis reaction is [28]

$$\begin{aligned}(2-2x)Y(NO_3)_3 + 2x\,RE(NO_3)_3 + 5(NH_2)_2CO \\ \longrightarrow (Y_{1-x}RE_x)_2O_3 + 5CO_2 + 8N_2 + 10\,H_2O.\end{aligned} \quad (1)$$

Nanocolloidal samples of Y_2O_3, $Y_2O_3:Eu^{3+}$, Tb^{3+}, $Y_2O_3:Tm^{3+}$ with different Eu^{3+} concentrations of 1, 3, 5, 7, and 10 mol%, Tb^{3+} concentration of 1.25 mol%, and Tm^{3+} concentrations of 1–4 mol% were prepared by a direct precipitation route from high-boiling polyol solution [22]. The starting materials were YCl_3, $EuCl_3$, $TbCl_3$, $TmCl_3$, NaOH, and diethylene glycol (DEG) with high purity grade.

The samples were checked by the X-ray diffractometer (D5000, Siemens). The morphology and particle sizes of $Y_2O_3:RE^{3+}$ were observed by transmission electron microscopy (TEM, H7600, Hitachi), high-resolution transmission electron microscopy HRTEM Philips CM200, 160 KV, and FE-SEM (S4800, Hitachi). Photoluminescent measurements were performed using a Jobin Yvon HR 460 monochromator and a multichannel CCD detector from instruments SA model Spectraview-2D for the visible and near infrared range and a Triax 320 with a PDA multichannel 256 pixels detector for the IR range. The decay time was analyzed by a PM Hamamatsu R928 and Nicolet 490 scope with a time constant of the order of 7 nanoseconds. Kimmon He-Cd laser (325 nm excitation), Nitrogen laser (337.1 nm), and Diode laser or Ti-Sapphire laser were used as the excitation sources.

3. RESULTS AND DISCUSSION

3.1. Morphology and structure of nanopowders and nanocolloidal media

Figure 1 shows TEM and HRTEM images of Y_2O_3 nanocolloidal and electron diffraction of Y_2O_3 nanoparticles. One can notice that our samples are spherical shaped, small sized (5 nm), and with narrow distribution.

The synthesis of useful amounts of sub 5 nm size lanthanide-doped oxides remains a challenge in optical material research. A few weeks ago, stable colloidal was prepared and has been reported in [22]. For the first time, nanocolloidal codoped Tb^{3+} and Eu^{3+} and oxide particle suspension were prepared in our laboratory. The transparent suspensions of particles dispersed in organic solvent were obtained with high stability for a year. The absorption spectra of the colloids have been characterized with a strong and broad band for Y_2O_3, $Y_2O_3:Eu^{3+}$, $Y_2O_3:Tb^{3+}$, $Y_2O_3:Tm^{3+}$, $Y_2O_3:Eu^{3+}$, Tb^{3+} nanoparticles in the long range from 230 nm to 380 nm with the maxima around 240–250 nm.

X-ray diffraction of $Y_2O_3:RE^{3+}$ samples annealed at different temperatures was studied. The pure polycrystalline Y_2O_3 was used as standard sample for the correction of the instrumental line broadening. The profiles of diffracting peaks were fitted to the ps-voigt1 function. The grain sizes and size distribution have been determined by the WINCRYSIZE program packet [40]. The column length distribution can be obtained from double differentiation of the Fourier transform of the line profile [41]. According to this method, the reflection intensity of the given set of lattice planes is expressed in terms of a sum of the intensities from all columns of lattice cells perpendicular to the planes [42, 43].

Figure 2 exhibits X-ray diffraction (XRD) patterns of $Y_2O_3:Eu^{3+}$ (5%) annealed at 500, 550, 600, 700, and 900°C. The powder annealed at 500°C is amorphous. The Y_2O_3 cubic phase appears when annealed above 550°C.

The main diffraction peaks, in agreement with the JCPDS 41-1105 reference, correspond to the [222], [400], [440], and [622] planes. However, the widths of the diffraction lines are

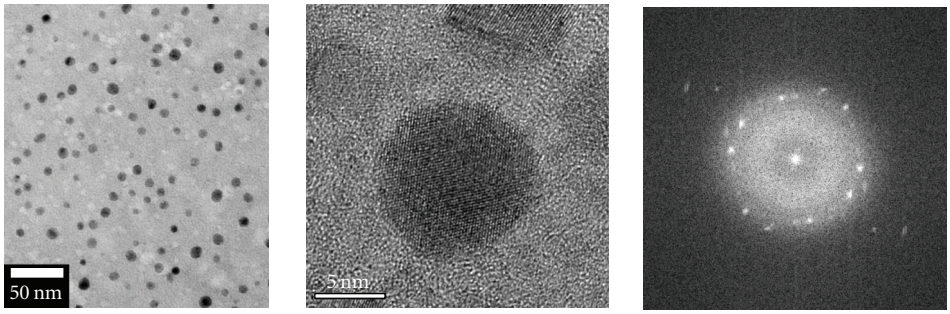

(a) (b) (c)

Figure 1: (a) TEM, (b) HRTEM images of Y_2O_3 nanocolloidal, and (c) the corresponding electron diffraction pattern of Y_2O_3 nanoparticles.

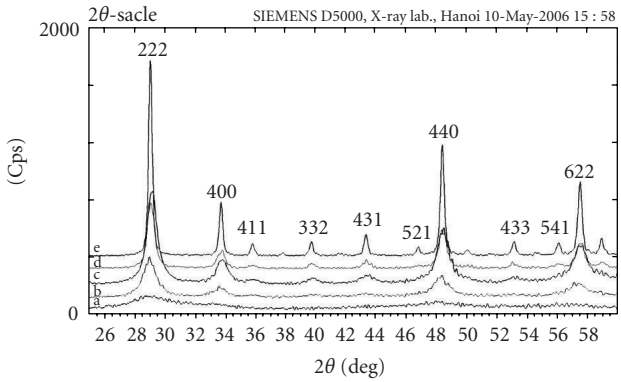

Figure 2: (a) XRD diffraction pattern of Y_2O_3:Eu^{3+} (5 mol%) powders annealed at 500°C, (b) 550°C, (c) 600°C, (d) 700°C, and (e) 900°C.

broadened because of the small size of the crystallites. Then they get narrower and narrower at higher temperatures. This process reflects the fact that the crystalline size is increasing with temperature of annealing process. The peak profiles of [222] reflection (in Figure 2, at $2\theta = 29.150$) were used for starting data of Warren-Averbach method [41]. This method was used to study nanocrystalline gold [42]. It was noted that the results of the average column length usually differ from crystallite sizes evaluated from Scherer equation [43]. The main reason is due to the Warren-Averbach method which provides a volumetric average of the crystallite size. We can see that the size distributions for small grains <10 nm have asymmetrical shape with small FWHM (of the size distribution), while for bigger grains they become more symmetrical and their FWHM are larger. The size distribution of Y_2O_3:Eu^{3+} (5%) versus annealing temperature and time calculated by Warren-Averbach method is presented in Table 1 and Figure 3.

The XRD of Y_2O_3:Er^{3+} 10 mol% nanomaterials (annealed at 600°C for 30 minutes) also shows a cubic symmetry like the Y_2O_3 reference powder. The FWHM of the diffraction lines for nanomaterials is larger than that of the Y_2O_3 crystals. The sizes are about 7 nm and 23.4 nm, respectively, the FWHM of the size distribution for the nanopowder is 11 nm and 20.1 nm for the sample annealed at 600°C for 30 minutes and at 800°C for 30 minutes, respectively. These data were also calculated by using the Warren-Averbach method. For the Y_2O_3:Tm^{3+} nanophores, the mean sizes of the particle are 7.2, 7.4, and 7.7 nm, respectively, with Tm^{3+} concentrations of 0.1, 1, and 4 mol%.

Table 1: Size and FWHM of Y_2O_3:Eu^{3+} particles versus annealing temperature and time.

T (°C)	Time (min)	d (nm)	FWHM (nm)
550	60	4.4	7.3
600	30	5.6	6.9
700	30	15.2	9.3
900	30	46.1	20.6
900	60	72.2	22.6

3.2. Luminescent spectra

Size-dependent efficiency was reported in Tb-doped Y_2O_3 nanocrystalline phosphor [11]. In Y_2O_3:Tb^{3+} nanocrystalline, the efficiency varied as the square of the particle size ranged from 100 to 40 Å. It could be nonradiative contributions decrease with the decrease in particle size. On the other hand, effects of grain size from 43 nm to 71 nm on wavelength of Y_2O_3:Eu^{3+} emission spectra are investigated in detail [12]. The blue shift effect of emission was observed very small in Y_2O_3:Eu^{3+} nanophosphor. In contrast, we could not find any blue shift change in the luminescent spectra of Y_2O_3:Eu^{3+} prepared by combustion reaction.

The photoluminescent (PL) spectra of Y_2O_3:Tb^{3+} nanocolloidal correspond to the $^5D_4$-^7F_J transitions according to the energy diagram and fluorescence processes of Tb^{3+} [5] (Figure 4(a)).

The PL spectra of Y_2O_3:Eu^{3+} nanocolloidal with different concentrations (from 1 to 10 mol%) under 337.1 nm N_2 laser excitation show narrow emission peaks corresponding to the $^5D_0$-^7F_J ($J = 0, 1, 2, 3, 4$) transitions of Eu^{3+}, with the most intense peak at 611 nm for the case of $J = 2$. Figure 4(b) presents the luminescent spectra of Y_2O_3-doped 1, 3, 5, 7, and 10% Eu^{3+} nanocolloidal under 337.1 nm N_2 laser excitation. The PL spectra of Y_2O_3:Eu^{3+} nanocolloidal also indicate

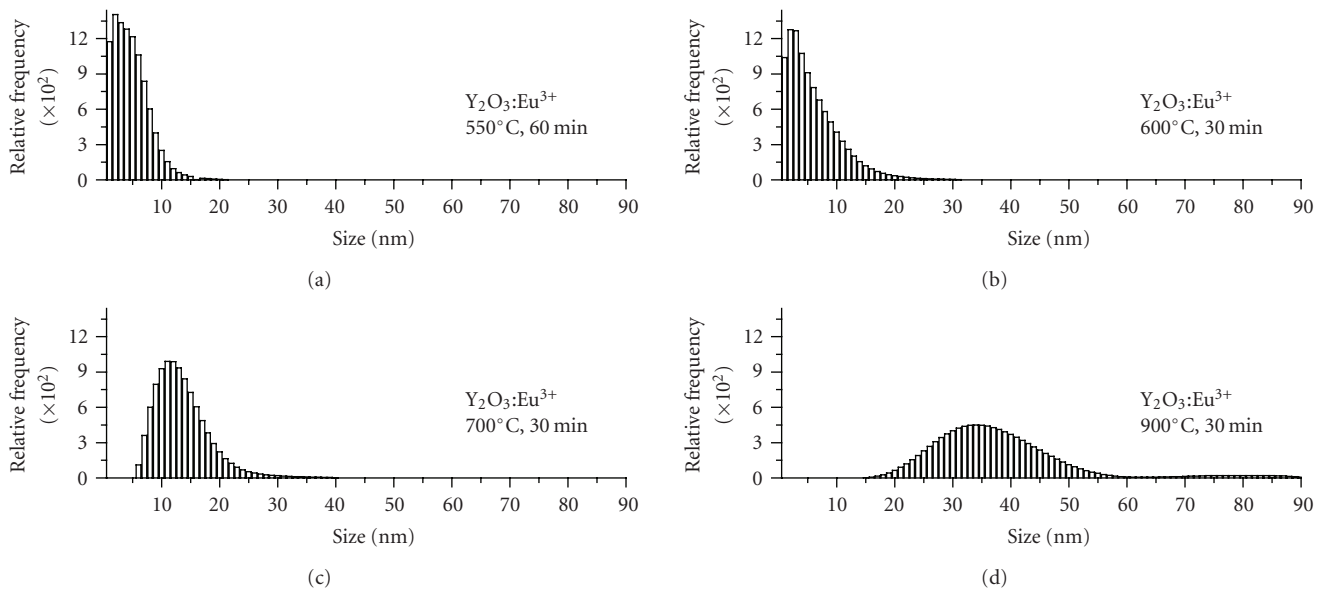

Figure 3: Size distribution calculated by W-A method of Y_2O_3:Eu^{3+} (5%) powder annealed in 30 minutes at the temperatures of 550°C, 600°C, 700°C, and 900°C.

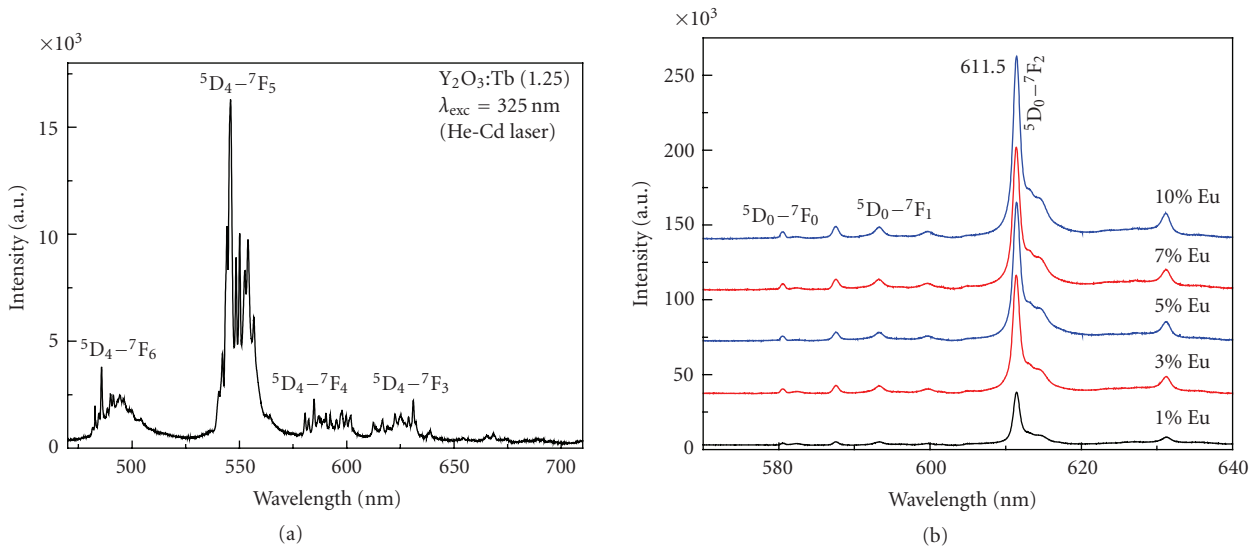

Figure 4: (a) Luminescent spectra of Y_2O_3:Tb^{3+} nanoparticles excited at 325 nm, (b) luminescent spectra of Y_2O_3 doped 1% Eu, 3% Eu, 5% Eu, 7% Eu, and 10% Eu nanoparticles (from colloidal) excited by N_2 laser at 337.1 nm.

that not any quenching of the PL intensity for Eu^{3+} concentration up to 10 mol%. Y_2O_3 presents a cubic structure with lattice constant a = 1.0604 Å. The primitive unit cell contains 80 atoms (48 O and 32 Y), Y atoms occupy two sites with the C_2 and $S_6(C_{3i})$ symmetry site. Our samples of Y_2O_3:Eu^{3+} nanopowder and nanocolloidal present a clearly dominant typical C_2 symmetry site.

For the Y_2O_3:Tm^{3+} phosphor, luminescent intensity is stronger and synthesis temperature is lower in the case of nanocolloidal than in the powder's one. From excited luminescence spectra one can notice that optimal intensity was observed when excited by 362 nm. The luminescent spectra of Y_2O_3:Tm^{3+} nanopowder under 362 nm excited were presented in Figure 5.

The spectra of nanocolloidal and nanopowder under 337.1 nm excited are presented in the inset of Figure 5. The position is not different, but the spectral resolution in the nanocolloidal seems to be better in the powder.

The nanocolloidals have a narrow size distribution and these spherical particles in the size range 5–10 nm are easy to mix with water or polymer solution. That can explain why the quenching concentration of Eu^{3+}, Tm^{3+}, and Er^{3+} has been raised remarkably. This nanocolloidal media is useful for preparing optical thin films.

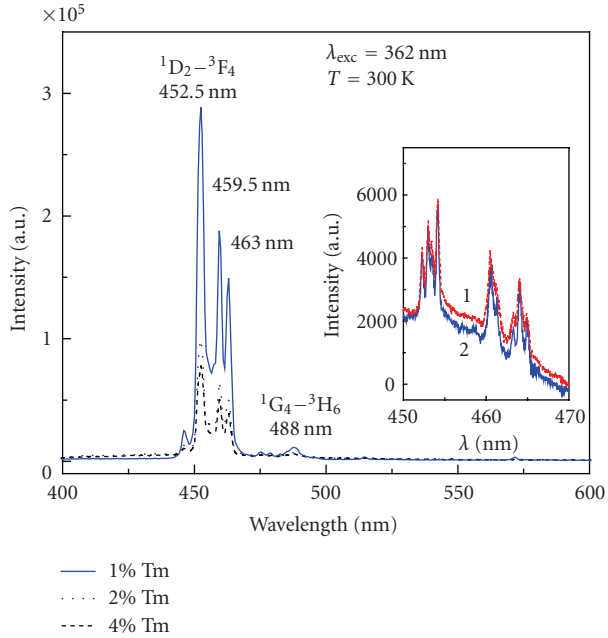

Figure 5: Luminescent spectra in dependence on Tm^{3+} concentration in Y_2O_3:Tm^{3+} (1, 2, 4 mol%) nanopowder under 362 nm excitation. Inset: luminescent spectra of Y_2O_3:Tm^{3+} nanocolloidal (1) and nanopowder (2) under 337.1 nm excitation.

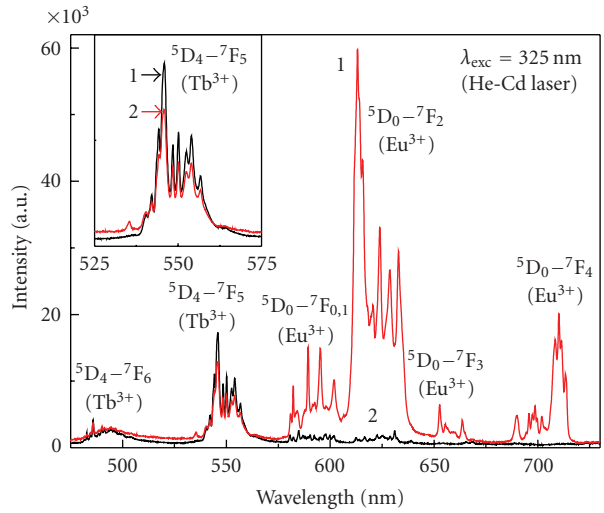

Figure 6: Luminescent spectra of Y_2O_3:1.25%Tb^{3+} (1) and Y_2O_3:1.25%Tb^{3+}, 5%Eu^{3+} (2) nanocolloidal excited by He-Cd laser at 325 nm, inset to compare intensity of Tb^{3+} in Y_2O_3:1.25%Tb^{3+} and Y_2O_3:1.25%Tb^{3+}, 5%Eu^{3+}.

3.3. Energy transfer and upconversion mechanisms

The role of concentration, temperature, solvents as well as upconversion, and ET mechanism were investigated in detail for Y_2O_3 nanophores containing Eu^{3+}, Tb^{3+}, Er^{3+}, and Yb^{3+} rare earth ions [34]. ET between Tb^{3+} and Eu^{3+} in nanopowder has been elucidated from the luminescent spectra of $(Y_{0.95}Eu_xTb_y)_2O_3$ (with x/y = 8/2, 9/1, 7/3) by Anh et al. in our previous paper [28]. In Y_2O_3:Tb^{3+}, Eu^{3+} sample, the spectra exhibits the well-known $^5D_0$-^7F_J line emissions ($J = 0, 1, 2, \ldots$) of the Eu^{3+} ion with the strongest line for $J = 2$ at 612 nm in the red region. The peak at 546 nm assigned to the $^5D_4$-$^7F_5$ transition of Tb^{3+} ions is also observed. But the intensity of this peak is much lower than the peak corresponding to the $^5D_0$-$^7F_2$ transition of Eu^{3+}. The peak at 546 nm was also lower for the Eu^{3+} and Tb^{3+} codoped sample than the Tb^{3+} doped one. One can notice that the emission spectra of Tb^{3+} in Y_2O_3 nanocrystal are slightly quenched by Eu^{3+} ions due to energy transfer from Tb^{3+} to Eu^{3+}. The luminescent spectra of Y_2O_3:Tb^{3+} (1.25%), Eu^{3+} (5%), and Y_2O_3:Tb^{3+} (1.25%) nanocolloidals are shown in Figure 6. The intensity of the Eu^{3+} emission based on energy transfer from Tb^{3+} was analyzed in previous papers [28, 32].

Under 980 nm irradiation, upconversion spectra in the visible range from 500 nm–700 nm of Y_2O_3 : Er^{3+} (dash dot line) and Y_2O_3:Er^{3+}, Yb^{3+} (solid line) are presented in Figure 7(a). The Er^{3+}-Er^{3+} upconversion mechanism is explained in accordance with the energy schema (Figure 7(b), right). There is a great interest in the use of upconversion materials for efficient conversion of infrared radiation to visible light. This phenomenon has applications in several areas, such as upconversion lasing, and two photons fluorescence imaging, cathodoluminescence, and other applications. The Er^{3+} ion finds uses in laser materials and optical amplifiers under ground- and excited-state transitions near 800 and 980 nm, where high-power diodes are available [5]. In Y_2O_3:Er^{3+} nanophosphor, the green and red fluorescence lines are observed in our samples after 800 nm excitation, owing to the transitions ($^2H_{11/2}$,$^4S_{3/2}$) → $^4I_{15/2}$ (515–575 nm) and $^4F_{9/2}$ → $^4I_{15/2}$ (640–690 nm) [26, 34]. Under 980 nm irradiation, the Er^{3+} ion is excited to the $^4F_{7/2}$ state via two successive energy transfers. An NIR photon from the pump beam will excite an Er^{+3} ion from the $^4I_{15/2}$ ground state to the $^4I_{11/2}$ state. Another Er^{3+} ion also in the $^4I_{11/2}$ state and in close proximity will transfer its energy to the initial ion, thereby exciting it to the $^4F_{7/2}$ state. The lower emitting levels are then populated via multiphonon relaxation and green and red emissions are then observed.

Interactions between two Er^{3+} ions cannot be ignored. Following the addition of Yb^{3+} ions, this process is greatly diminished due to the large absorption cross-section of the Yb^{3+} ions. The Er^{3+} absorption cross-section at this 980 nm wavelength is not very high. By the addition of Yb^{3+}, pumping promotes an electron from the $^2F_{7/2}$ ground state to the $^2F_{7/2}$ manifold of Yb^{3+}; the excited Yb^{3+} ion then transfers its energy to the Er^{3+} $^4I_{11/2}$ level (Figure 7(b)).

Since the population of the $^4I_{13/2}$ level was increased, the lifetime was also increased. Two deleterious processes can also occur: via back energy transfer from Er^{3+} to Yb^{3+} ions, or double energy transfer, where a second excited Yb^{3+} ion transfers its energy to the Er^{3+} ion and promotes one electron from the $^4I_{11/2}$ to the $^4F_{7/2}$. When the Yb^{3+} concentration is enhanced, the Er^{3+} ions start to "see" Yb^{3+} ions and deleterious $Er^{3+} \leftrightarrow Er^{3+}$ energy exchanges are progressively replaced by the beneficial $Yb^{3+} \leftrightarrow Er^{3+}$ transfers.

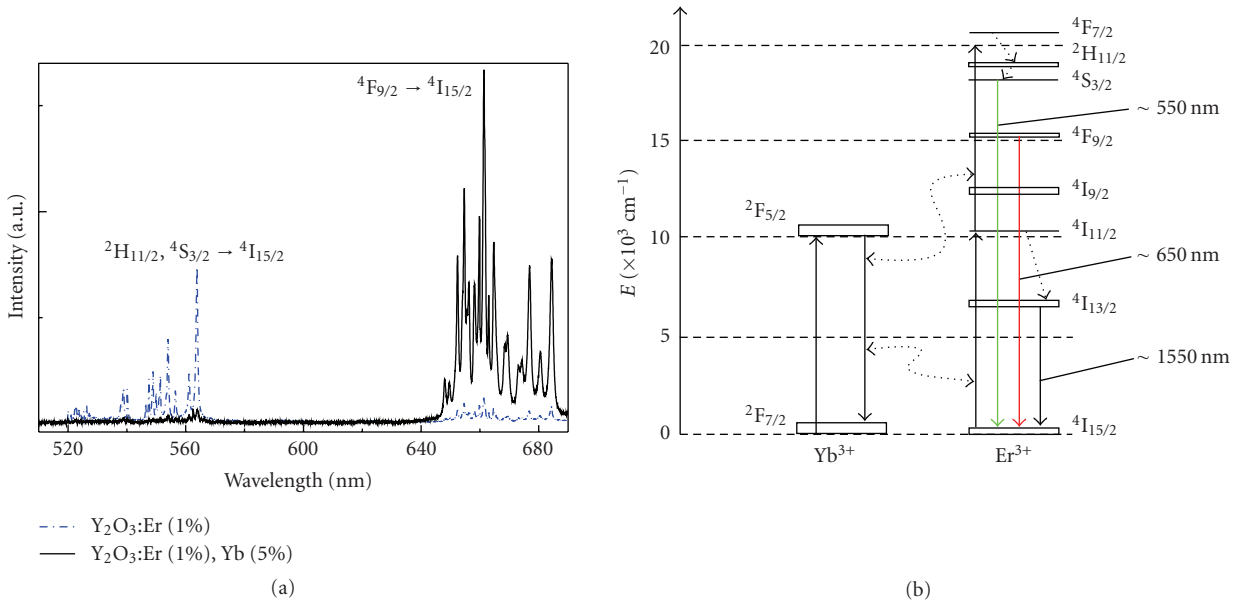

Figure 7: (a) Upconversion spectra in the visible range from 500 nm to 700 nm of Y_2O_3:Er^{3+} (dash doted line) Y_2O_3:Er^{3+}, Yb^{3+} (solid line) following 980 nm irradiation, (b) energy schema presented the upconversion fluorescence interacted between Er-activator and Yb-sensitizer.

Comparing codoped Y_2O_3:Er^{3+}, Yb^{3+} nanophosphors with Er^{3+} concentration varying from 0.1 to 5 mol% and 5 mol% Yb^{3+}, the optimal content for the luminescent intensity at 1538 nm ($^4I_{13/2}$-$^4I_{15/2}$ transition) is 1 mol% Er^{3+}. The upconversion in the red region 640–675 nm presents also a maximum for 1 mol% Er^{3+}. The effect of Er^{3+} concentration on upconversion luminescence of Y_2O_3:Er^{3+}, Yb^{3+} is complicated depending on the power of the excitation laser. Red upconversion luminescence is caused by a two-photon process, when excitation power is high enough, as to the samples with lower concentration of Er^{3+} the intensity of green light is weaker than that of red light because more ions will nonradiatively decay from higher levels to $^2H_{11/2}$ and $^4S_{3/2}$ levels [30].

An advantage offered by our nanophosphors over the two-photon excitable organic dye is that the upconversion process in the Y_2O_3:Er^{3+}, Yb^{3+} nanophosphor occurs by sequential multistep absorption through real states and is thus considerably stronger. One can use a low-power continuous wave diode laser in the near infrared region to excite the upconverted emission. By contrast, the two photon absorption in organic dyes that is directed (simultaneous) requires a high-peak power pulse laser source for two-photon absorption through a virtual state. Figure 8 shows the luminescent intensities of the band at 564 nm and 1538 nm versus the excitation power at 803.7 nm of a diode laser.

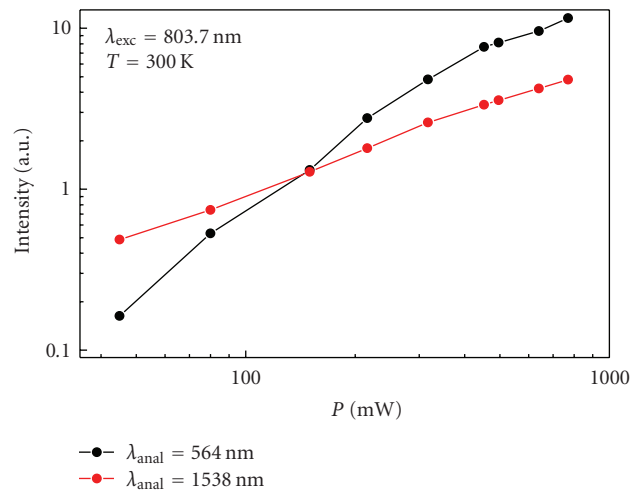

Figure 8: Luminescent intensities of the band at 564 nm and 1538 nm versus the excitation power at 803.7 nm.

3.4. Study energy transfer based on the decay times of fluorescence

The decay curves of Eu^{3+} and Tb^{3+} of Y_2O_3:Eu^{3+}, Tb^{3+} nanopowders for Eu^{3+}/Tb^{3+} = 9/1, 8/2, and 7/3, respectively, (for 5 mol% rare earth ions) are presented in Figure 9(a) (Eu^{3+} emission at 612 nm) and Figure 9(b) (Tb^{3+} emission at 546 nm). The decay curves being nonexponential, we have considered the normalized area S_N under the decay curve. The lifetimes of Eu^{3+} are 940, 360, and 650 microseconds for the case Eu^{3+}/Tb^{3+} = 9/1, 8/2, and 7/3, respectively. The lifetimes of Tb^{3+} decreased from 400 microseconds to 175 microseconds for the case Eu^{3+}/Tb^{3+} = 9/1, 8/2, respectively, by ET process.

The results have indicated that the ratio between Eu^{3+}/Tb^{3+} plays an important role in the ET process. The most effective ET is clearly for the sample with Eu^{3+}/Tb^{3+} ratio of 8/2. The ET between Tb^{3+} and Eu^{3+} has been also investigated in Y_2O_3 crystals [4] and in $Tb_{1-x}Eu_xP_5O_{14}$ crystals [44]. Site-selective spectra and time-resolved spectra

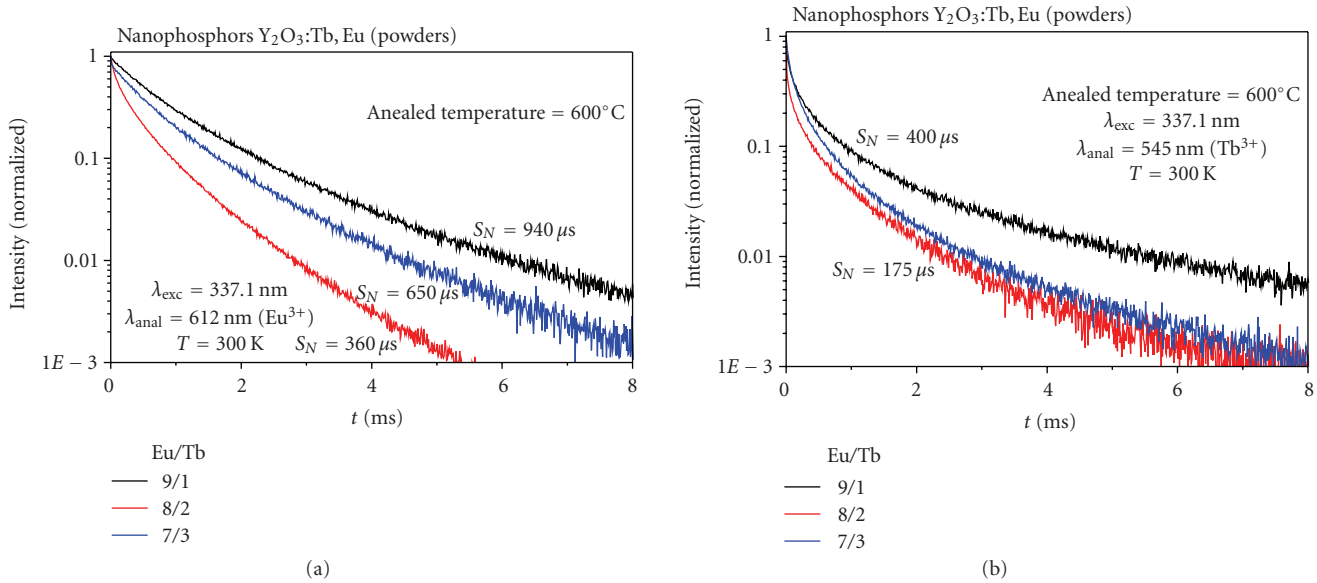

Figure 9: Decay curves at wavelength of 611 nm for Eu^{3+} (a) and of 545 nm for Tb^{3+} (b) in Y_2O_3:Eu^{3+}, Tb^{3+} (5%) nanophosphor, annealed at 600°C, in 30 minutes.

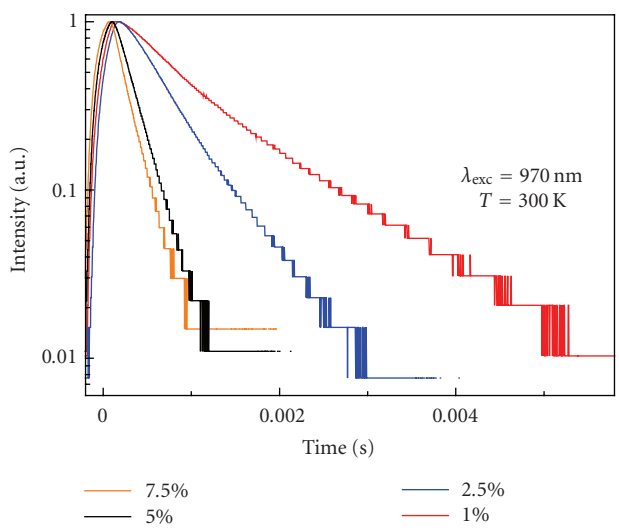

Figure 10: Decay curves for the band at 1535 nm of Y_2O_3:Er^{3+} nanophosphor versus Er^{3+}-concentration, under excitation at 970 nm.

of Y_2O_3:Eu^{3+} nanocrystal were investigated [45]. Recently, Hongei Song studies the dependence of photoluminescent properties of cubic Y_2O_3:Tb^{3+} nanocrystal on particles size and temperature [46]. Up to now, our group is the only group which has studied energy transfer between Tb^{3+}-Eu^{3+} in nanophosphors (powder and colloidal) of Y_2O_3 codoped with Tb^{3+}-Eu^{3+}.

In studying the decay behavior of the infrared emission of the $^4I_{13/2}$-$^4I_{15/2}$, transitions of Er^{3+} at 1535 nm depending on the Er-concentration from 1, 2.5, 5, 7, 5, 10, up to 15 mol% have been measured for Y_2O_3:Er^{3+} phosphor and presented in Figure 10. Under 970 nm excitation, the decay times are not purely exponential. There are two kinds of lifetimes: the short lifetimes are 250, 150, 35, and 15 microseconds in the case of 1%, 2.5%, 7.5%, and 15% Er; the second long lifetime decreases from 1300, 620, and 110 microseconds to 80 microseconds, respectively. The lifetime of the emission IR increases as the concentration decreases. As for luminescence, it would be interesting to obtain a series of samples prepared under the same conditions and having undergone more significant temperatures of annealing, one could then determine the temperature from which one observes effects extinction. Lastly, let us note that the results of the spectra and the decays are coherent between them.

3.5. Application potential

Flat panel displays (FPDs) are thinner, lighter, and consume less than the conventional cathode-ray tube (CRT) displays. The field emission displays (FEDs) are the most promising FPDs technology. Rare earth-yttrium oxide is one of the important materials for application not only for FEDs, but also for waveguide and laser host. Enhancement of cathodoluminescent and photoluminescent properties of Y_2O_3:Eu^{3+} luminescent films by vacuum cooling were observed [47], structural and optical properties of rare-earth-doped Y_2O_3 waveguides grown by pulsed-laser deposition were studied [48]. Growth of rare earth (RE-) doped concentration gradient crystal fibers and analysis of dynamical processes of laser resonant transitions in RE-doped Y_2O_3 (RE = Yb^{3+}, Er^{3+}, Ho^{3+}) were also studied [49]. Nanostructured ZnO/Y_2O_3:Eu^{3+} for use as in luminescent polymer electrolyte composites was presented [50]. Thin films were prepared [51, 52] in order to apply for FPDs. The upconverting nanophores for bioimaging were presented in detail by Prasad [53]. The lifetimes of the nanophosphors

contained rare-earth ions in the range of millisecond and microsecond are compared to organic dye fluorescence with a lifetime typically in nanosecond. Specially, in our institute infrared cards were successfully proposed by mixing Y2O3:Er^{3+}, Yb^{3+}, or Y2O3:Er^{3+} with polymethylmethacrylate (PMMA) with active imaging area of $20 \times 20\,mm^2$. These cards allow to detect a diode laser emitting at 980 nm with power of $7\,mW/cm^2$. The red (655 nm–675 nm) or the green (520 nm–570 nm) emissions could be observed in depending on the concentration of Er-Yb couple. They are stable under 980 nm irradiation in the tropical conditions with humidity near to 90%. The optical coding systems based on the nanophosphors with ET luminescent and upconversion effect contained Eu^{3+}-Tb^{3+} (excitedby UV light at 370, 365, 337.1, and 325 nm) and Er^{3+}-Yb^{3+} activators (excited by diode laser at 800 nm, 980 nm) have been successfully developed for examination of commercial products, banknote [28, 54, 55], nanobarcodes [53], or planar waveguide [56].

4. CONCLUSIONS

In this paper, we have presented two simple and efficient methods to prepare highly luminescent Y_2O_3 nanophosphor doped with Eu^{3+}, Tb^{3+}, Tm^{3+}, Er^{3+}, and Yb^{3+}. The average size and its distribution of the nanophosphor can be tailored sharply in nanoscale.

The optical properties and photophysic process, especially ET in Y_2O_3 host matrix, have been investigated and elucidated for improving the luminescence and upconversion processes.

Y_2O_3 nanophosphor in colloidal media with averaged size of 5 nm, narrow distribution, and spherical shape was successfully prepared. The colloidal are transparent and well stable at the concentration of 10%. The luminescence was strong and energy transfer was observed in Y_2O_3:Tb^{3+}, Eu^{3+}. The upconversion emission from Y_2O_3:Er^{3+}, Yb^{3+} nanophosphor is remarkable for developing an infrared display card. Y_2O_3:Tm^{3+} together with both Y_2O_3:Tb^{3+}, Eu^{3+} and Y_2O_3:Er^{3+}, Yb^{3+} is good candidate for interesting application such as infrared cards and coding cards or biosensors. The transparent colloidal could be a promising approach for fabricating an optoelectronic thin film with higher optical quality.

ACKNOWLEDGMENTS

The authors would like to thank Professor Nguyen Van Hieu for his help, National Project for Advanced Materials Science and Technology, no. KC.02.14, National Nanoprogram 810304, the Basis research state projects of CB20 and Program for application of nanophosphors of Vietnamese Academy of Science and Technology 2007-2008 KHCN (financially supported this work). A part of the authors work was done in the National Key Laboratory of Electronic Materials and Devices, Institute of Materials Science, and Vietnamese Academy of Science and Technology.

REFERENCES

[1] C. Feldmann, T. Jüstel, C. R. Ronda, and P. J. Schmidt, "Inorganic luminescent materials: 100 years of research and application," *Advanced Functional Materials*, vol. 13, no. 7, pp. 511–516, 2003.

[2] A. S. Edelstein and R. C. Cammarata, Eds., *Nanomaterials: Synthesis, Properties and Applications*, Taylor & Francis, London, UK, 1998.

[3] B. R. Ratna, A. D. Dinsmore, et al., "Nanophosphors: synthesis, properties and application," in *Proceedings of the 5th International Conference on the Science and Technology of Display Phosphors (ICSTDP '99)*, p. 295, San Diego, Calif, USA, November 1999.

[4] T. K. Anh, T. Ngoc, P. T. Nga, V. T. Bich, P. Long, and W. Strek, "Energy transfer between Tb^{3+} and Eu^{3+} in Y_2O_3 crystals," *Journal of Luminescence*, vol. 39, no. 4, pp. 215–221, 1988.

[5] S. Shionoya and W. M. Yen, *Phosphor Handbook*, CRC Press, Boca Raton, Fla, USA, 1999.

[6] G. Blasse and B. C. Grabmaier, *Luminescent Materials*, Springer, Berlin, Germany, 1994.

[7] H. Eilers and B. M. Tissue, "Laser Spectroscopy of Nanocrystals Eu_2O_3 and Eu^{3+}:Y_2O_3," *Chemical Physics Letters*, vol. 251, no. 1-2, pp. 74–78, 1996.

[8] M. Kottaisamy, D. Jeyakumar, R. Jagannathan, and M. M. Rao, "Yttrium oxide: Eu^{3+} red phosphor by self-propagating high temperature synthesis," *Materials Research Bulletin*, vol. 31, no. 8, pp. 1013–1020, 1996.

[9] B. Bihari, H. Eilers, and B. M. Tissue, "Spectra and dynamics of monoclinic Eu_2O_3 and Eu^{3+}:Y_2O_3 nanocrystals," *Journal of Luminescence*, vol. 75, no. 1, pp. 1–10, 1997.

[10] T. Ye, Z. Guiwen, Z. Weiping, and X. Shangda, "Combustion synthesis and photoluminescence of nanocrystalline Y_2O_3:Eu phosphors," *Materials Research Bulletin*, vol. 32, no. 5, pp. 501–506, 1997.

[11] E. T. Goldburt, B. Kulkarni, R. N. Bhargava, J. Taylor, and M. Libera, "Size dependent efficiency in Tb doped Y_2O_3 nanocrystalline phosphor," *Journal of Luminescence*, vol. 72–74, pp. 190–192, 1997.

[12] Q. Li, L. Gao, and D. Yan, "Effects of grain size on wavelength of Y_2O_3:Eu^{3+} emission spectra," *Nanostructured Materials*, vol. 8, no. 7, pp. 825–831, 1997.

[13] J. A. Cooper, H. G. Paris, S. R. Stock, C. J. Summers, and D. N. Hill, "Investigation of the effect of process variables on properties of europium-doped yttrium-oxide phosphor," *Journal of the Society for Information Display*, vol. 6, no. 3, pp. 163–166, 1998.

[14] D. K. Williams, B. Bihari, B. M. Tissue, and J. M. McHale, "Preparation and fluorescence spectroscopy of bulk monoclinic Eu^{3+}:Y_2O_3 and comparison to Eu^{3+}:Y_2O_3 nanocrystals," *Journal of Physical Chemistry B*, vol. 102, no. 6, pp. 916–920, 1998.

[15] A. Konrad, T. Fries, A. Gahn, et al., "Chemical vapor synthesis and luminescence properties of nanocrystalline cubic Y_2O_3:Eu," *Journal of Applied Physics*, vol. 86, no. 6, pp. 3129–3133, 1999.

[16] T. K. Anh, N. Vu, P. T. M. Chau, L. Q. Minh, N. T. Oanh, and C. Barthou, "Preparation and optical properties of Y_2O_3:Eu nanophosphors," in *Proceedings of the 3rd International Workshop on the Materials Science*, F. F. Bekker, N. D. Chien, J. J. M. Franse, T. D. Hien, N. T. Hien, and N. P. Thuy, Eds., Trends in Materials and Technology, pp. 320–323, Hanoi, Vietnam, November 1999.

[17] J. A. Capobianco, F. Vetron, T. D'Alesio, G. Tessari, A. Speghini, and M. Bettinelli, "Optical spectroscopy of nanocrystalline cubic Y_2O_3:Er^{3+} obtained via combustion synthesis," *Physical Chemistry Chemical Physics*, vol. 2, pp. 3203–3207, 2000.

[18] J. Zhang, Z. Zhang, Z. Tang, Y. Lin, and Z. Zheng, "Luminescent properties of Y_2O_3:Eu synthesized by sol-gel processing," *Journal of Materials Processing Technology*, vol. 121, no. 2-3, pp. 265–268, 2002.

[19] G. Y. Hong, B. S. Jeon, Y. K. Yoo, and J. S. Yoo, "Photoluminescence characteristics of spherical Y_2O_3:Eu phosphors by aerosol pyrolysis," *Journal of the Electrochemical Society*, vol. 148, no. 11, pp. H161–H166, 2001.

[20] T. Igarashi, M. Ihara, T. Kusunoki, K. Ohno, T. Isobe, and M. Senna, "Relationship between optical properties and crystallinity of nanometer Y_2O_3:Eu phosphor," *Applied Physics Letters*, vol. 76, no. 12, pp. 1549–1551, 2000.

[21] C. Feldmann, "Polyol-mediated synthesis of nanoscale functional materials," *Advanced Functional Materials*, vol. 13, no. 2, pp. 101–107, 2003.

[22] R. Bazzi, M. A. Flores-Gonzalez, C. Louis, et al., "Synthesis and luminescent properties of sub-5-nm lanthanide oxides nanoparticles," *Journal of Luminescence*, vol. 102-103, pp. 445–450, 2003.

[23] G. Wakefield, E. Holland, P. J. Dobson, and J. L. Hutchison, "Luminescence properties of nanocrystalline Y_2O_3:Eu," *Advanced Materials*, vol. 13, no. 20, pp. 1557–1560, 2001.

[24] T. K. Anh, "The role of active centre concentration in the phenomena of energy transfer in lanthanide compounds," Doctoral thesis, Wroclaw-Warsaw, Poland, 1987.

[25] D. R. Tallant, C. H. Seager, and R. L. Simpson, "Energy transfer and relaxation in europium-activated Y_2O_3 after excitation by ultraviolet photons," *Journal of Applied Physics*, vol. 91, no. 7, pp. 4053–4064, 2002.

[26] N. Vu, T. K. Anh, L. Q. Minh, and C. Barthou, "Optical properties of Er^{3+} doped Y_2O_3 nanophosphors," *Communication in Physics*, vol. 12, pp. 119–123, 2002.

[27] T.-L. Phan, M. H. Phan, N. Vu, T. K. Anh, and S.-C. Yu, "Luminescent properties of Eu-doped Y_2O_3 nanophosphors," *Physica Status Solidi (a)*, vol. 201, no. 9, pp. 2170–2174, 2004.

[28] T. K. Anh, L. Q. Minh, N. Vu, et al., "Nanomaterials containing rare-earth ions Tb, Eu, Er and Yb: preparation, optical properties and application potential," *Journal of Luminescence*, vol. 102-103, pp. 391–394, 2003.

[29] N. Vu, T. K. Anh, C. Barthou, and L. Q. Minh, "Preparation, optical properties and up conversion effect of the nanophosphors doped with Er and Yb rare earth ions," in *Proceedings of the 9th Asia Pacific Physics Conference (APPC '04)*, pp. 579–580, Hanoi, Vietnam, October 2004.

[30] N. Vu, *Preparation, optical properties of nanophosphors Y_2O_3:Eu, Tb, Er and Yb*, Ph.D. thesis, Institute of Materials Science, Hanoi, Vietnam, 2007.

[31] N. Nguyen, M. H. Nam, T. K. Anh, L. Q. Minh, and E. Tanguy, "Optical properties of Eu^{3+} doped Y_2O_3 nanophosphors," *Advances in Natural Sciences*, vol. 6, pp. 119–123, 2006.

[32] T. K. Anh, L. T. K. Giang, N. Vu, et al., "Luminescence and energy transfer of Y_2O_3 nanocolloidal containing rare earth ions," *Journal on Science and Technology for Development*, vol. 24, pp. 85–93, 2007.

[33] N. Vu, T. K. Anh, G.-C. Yi, and W. Strek, "Photoluminescence and cathodoluminescence properties of Y_2O_3:Eu nanophosphors prepared by combustion synthesis," *Journal of Luminescence*, vol. 122-123, pp. 776–779, 2007.

[34] J. A. Capobianco, F. Vetrone, J. C. Boyer, A. Speghini, and M. Bettinelli, "Enhancement of red emission ($^4F_{9/2} \rightarrow {}^4I_{15/2}$) via upconversion in bulk and nanocrystalline cubic Y_2O_3:Er^{3+}," *Journal of Physical Chemistry B*, vol. 106, no. 6, pp. 1181–1187, 2002.

[35] D. Matsuura, "Red, green, and blue upconversion luminescence of trivalent-rare-earth ion-doped Y_2O_3 nanocrystals," *Applied Physics Letters*, vol. 81, no. 24, pp. 4526–4528, 2002.

[36] A. M. Pires, O. A. Serra, and M. R. Davolos, "Morphological and luminescent studies on nanosized Er, Yb-yttrium oxide up-converter prepared from different precursors," *Journal of Luminescence*, vol. 113, no. 3-4, pp. 174–182, 2005.

[37] F. Vetrone, J. C. Boyer, J. A. Capobianco, A. Speghini, and M. Bettinelli, "Effect of Yb^{3+} codoping on the up conversion emission in nanocrystalline Y_2O_3:Er^{3+}," *Journal of Physical Chemistry B*, vol. 107, no. 5, pp. 1107–1112, 2003.

[38] G. De, W. Qi, J. Zhang, et al., "Upconversion luminescence properties of Y_2O_3:Yb^{3+}, Er^{3+} nanostructures," *Journal of Luminescence*, vol. 119-120, pp. 258–263, 2006.

[39] C. Strohhöfer and A. Polman, "Absorption and emission spectroscopy in Er^{3+}-Yb^{3+} doped aluminum oxide waveguides," *Optical Materials*, vol. 21, no. 4, pp. 705–712, 2003.

[40] SIEMENS, *Profile User's Guide*, 1994, Diffrac-AT, Version 3.2.

[41] SIEMENS Win-Crysize, 1998.

[42] T. Inami, M. Kobiyama, S. Okuda, H. Maeta, and H. Ohtsuka, "Grain size measurement of nanocrystalline gold by X-ray diffraction method," *Nanostructured Materials*, vol. 12, no. 5–8, pp. 657–660, 1999.

[43] L. T. C. Tuong and P. V. Phuc, "Determination of nanocrystal-sizes and their distribution by X-ray diffraction method for Y_2O_3:Eu nanophosphors," in *Proceedings of the International Workshop on Optics and Spectroscopy*, pp. 501–504, Hanoi, Vietnam, March-April 2000.

[44] T. K. Anh and W. Strek, "Dynamics of energy transfer in $Tb_{1-x}Eu_xP_5O_{14}$ crystals," *Journal of Luminescence*, vol. 42, no. 4, pp. 205–210, 1988.

[45] H. Song and J. Wang, "Dependence of photoluminescent properties of cubic Y_2O_3:Tb^{3+} nanocrystals on particle size and temperature," *Journal of Luminescence*, vol. 118, no. 2, pp. 220–226, 2006.

[46] Z. Wei-Wei, X. Mei, Z. Wei-Ping, et al., "Site-selective spectra and time-resolved spectra of nanocrystalline Y_2O_3:Eu," *Chemical Physics Letters*, vol. 376, no. 3-4, pp. 318–323, 2003.

[47] D. Kumar, J. Sankar, K. G. Cho, V. Craciun, and R. K. Singh, "Enhancement of cathodoluminescent and photoluminescent properties of Eu:Y_2O_3 luminescent films by vacuum cooling," *Applied Physics Letters*, vol. 77, no. 16, pp. 2518–2520, 2000.

[48] O. Pons-Y-Moll, J. Perriere, E. Millon, et al., "Structural and optical properties of rare-earth-doped Y_2O_3 waveguides grown by pulsed-laser deposition," *Journal of Applied Physics*, vol. 92, no. 9, pp. 4885–4890, 2002.

[49] L. Laversenne, C. Goutaudier, Y. Guyot, M. Th. Cohen-Adad, and G. Boulon, "Growth of rare earth (RE) doped concentration gradient crystal fibers and analysis of dynamical processes of laser resonant transitions in RE-doped Y_2O_3 (RE=Yb^{3+}, Er^{3+}, Ho^{3+})," *Journal of Alloys and Compounds*, vol. 341, no. 1-2, pp. 214–219, 2002.

[50] M. Abdullah, C. Panatarani, T.-O Kim, and K. Okuyama, "Nanostructured ZnO/Y_2O_3:Eu for use as in luminescent polymer electrolyte composites," *Journal of Alloys and Compounds*, vol. 377, no. 1-2, pp. 298–305, 2004.

[51] N. Joffin, J. Dexpert-Ghys, M. Verelst, G. Baret, and A. Garcia, "The influence of microstructure on luminescent properties of Y_2O_3:Eu prepared by spray pyrolysis," *Journal of Luminescence*, vol. 113, no. 3-4, pp. 249–257, 2005.

[52] S.-S. Yi, J. S. Bae, B. K. Moon, J. H. Jeong, J.-C. Park, and I. W. Kim, "Enhanced luminescence of pulsed-laser-deposited Y_2O_3:Eu^{3+} thin-film phosphors by Li doping," *Applied Physics Letters*, vol. 81, no. 18, pp. 3344–3346, 2002.

[53] P. N. Prasad, *Nanophotonic*, Wiley-Interscience, New York, NY, USA, 2004.

[54] T. K. Anh, N. Vu, T. T. Huong, and L. Q. Minh, "Nanomaterials containing rare earth ions for infrared card and planar waveguide applications," in *The 2nd International Workshop on Nanophysics and Nanotechnology (IWONN '04)*, pp. 161–164, Hanoi, Vietnam, October 2004.

[55] T. K. Anh, L. T. K. Giang, L. D. Tuyen, et al., "Oxide nanoparticles and colloidal, preparation, optical properties and application potential," in *Proceedings of the 1st International Workshop on Functional Materials and the 3rd International Workshop on Nanophysics and Nanotechnology*, pp. 424–427, Halong, Vietnam, December 2006.

[56] T. T. Huong, T. K. Anh, M. H. Nam, C. Barthou, W. Strek, and L. Q. Minh, "Preparation and infrared emission of silica-zirconia-alumina doped with erbium for planar waveguide," *Journal of Luminescence*, vol. 122-123, pp. 911–913, 2007.